# Some operative applications of remote sensing

**Arnaldo Tonelli**
*Via Miramonti 4 - Rovereto (TN), Italy*

**Abstract**
Among the methods of applied geophysics, remote sensing plays a major and an ancillary role, at the same time. The major role deals with the acquisition and processing of data with the aim of describing the properties of the surfaces and their subsurface mass. The ancillary one consists in furnishing indications to address specific geophysical surveys. The paper presents some operative applications of remote sensing by stations fixed on ground and by airborne surveys: monitoring the biogas vents and evaluating their flow in waste disposal sites, analyzing the stability of rocky walls, studying the moisture content of soils for the most general purposes and in particular to contribute to archaeological prospecting. Single and multitemporal collection of data are taken into consideration to describe polarizing properties of the surfaces and to define the heat capacity in the thermal infrared domain and the presence of luminescent phenomena in the visible range. The use of environmental indicators, like vegetation, is also discussed with the aim of revealing through superficial seepages the pattern of underlying mass.

**Key words** *remote sensing – thermography – heat capacity – polarization – biogas detection – slope stability – archaeological prospecting – soil moisture*

## 1. Generalities on remote sensing

### 1.1. *Introduction*

The processing and interpretation of images, collected on targets under investigation, constitutes the field of application of remote sensing. The aim of this technique is to describe a specific theme or, more generally, to perform a diagnosis on a given environmental situation. The object's surface reflects, scatters, transmits and emits electromagnetic energy. Through the analysis of these phoenomena some properties of the objects themselves can be described. Within the most general field of environmental monitoring, the contribution of remote sensing can be presented with the help of fig. 1.

At the short wavelengths of ultraviolet, visible and near infrared the reflectivity of surfaces is studied. On the other hand, at the longer wavelength of thermal infrared the emission of electromagnetic energy is studied.

The surfaces can be classified based on their spectral response (the so called «spectral signature»), roughness, presence of luminescence and polarizing phoenomena. The mass underneath the surface is analysed from the point of view of heat capacity and heat conductivity.

Moreover, remote sensing can be passive or active, depending on the nature of the source of energization, if natural (like the sun) or artificial (like radar).

The data in different regions of the electromagnetic spectrum are collected using orbiting platforms, airborne platforms, ground fixed stations, and so forth, each system with its own characteristics.

*Mailing address*: Ing. Arnaldo Tonelli, Via Miramonti 4, 38068 Rovereto (TN), Italy; e-mail: artonelli@inwind.it

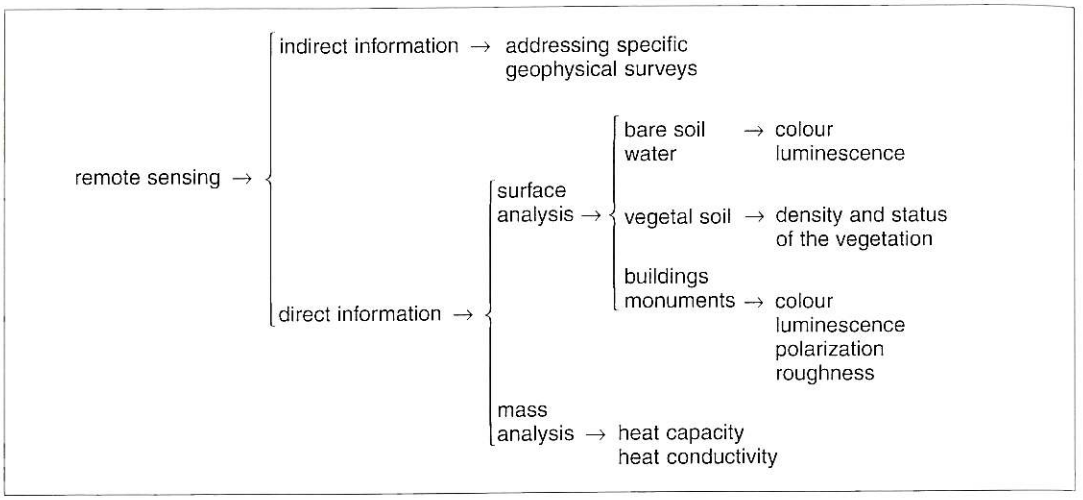


**Fig. 1.** Belonging to the family of geophysical methods and to the most general field of non destructive tests, remote sensing is applied to investigate shallow targets. Direct and indirect information can be acquired analysing some properties of the surface and subsurface mass.

### 1.2. *Wavelength intervals or spectral bands*

According to the Planck law, which describes the electromagnetic emission $E$ as a function of the absolute temperature $T$ and the wavelength $\lambda$,

$$E = C_1\lambda^{-5} / [\exp(C_2/\lambda T) - 1]$$

as well as the Wien displacement law, which defines the wavelength $\lambda_M$ of peack emission as a function of the absolute temperature $T$,

$$T[\mathrm{K}]\lambda_M[\mu\mathrm{m}] = 2898\ [\mathrm{K}\,\mu\mathrm{m}]$$

and the general expression, which describes the radiance $N_d$ collected by a sensor in function of the emissivity $\varepsilon$ of the surface observed, its emission as a black body $N_c$, and the radiance of an external illuminating source $N_s$

$$N_d = (1 - \varepsilon)N_s + \varepsilon N_c$$

sweeping the wavelengths, the predominant role of reflection or emission can be observed as the wavelength increases. At the short wavelength of ultraviolet (below 0.2 $\mu$m till 0.4 $\mu$m), visible (0.4 ÷ 0.7 $\mu$m) and near infrared (0.7 ÷ 1 $\mu$m) the reflection largely predominates over the emission, while in the domain of the longer wavelength of thermal infrared (8 ÷ 14 $\mu$m), the emission to a large extent predominates on the reflection. There exists a transitional zone (around 2.5 $\mu$m) where the two components can have a comparable weight. We can summarize the main properties of the most common spectral interval as follows:

*Ultraviolet (shorter than 0.2 $\mu$m to 0.4 $\mu$m)* – This is a spectral domain where the contrast among different targets is very low due to the severe scattering of the atmosphere. Its use is confined within short distances in the biosphere (while by the astronomers, working with satellites outside the atmosphere, the applications are numerous and promising). Ultraviolet can also detect oil slicks on water bodies and particular alterations on natural and artificial surfaces.

*Blue (0.4 ÷ 0.5 $\mu$m)* – In this region the scattering remains considerable and then the contrast low. Vegetation is seen as one of the most opaque natural bodies. Water is transparent. For these reasons the blue band is a good means by which to study, in a first approach, subaquatic vegetation.

*Green (0.5 ÷ 0.6 μm)* – Is a band of a general low contrast among the most common surfaces, limited scattering, maximum transparency for clear water. In this interval the vegetation reflects around 15% of the incident light.

*Red (0.6 ÷ 0.7 μm)* – The contrast increases, the transparency of water decreases, vegetation absorbs, in this spectral interval, the energy to activate photosynthesis (thus reflecting little, around 6%).

*Photographic infrared (0.75 ÷ 0.85 μm)* – A dramatic change appears crossing the boundary of the visible. Water transparency decreases even more: for this reason fresh snow from melting snow can be distinguished based on the relative opacity of this last one. Vegetation reflects strongly. Good contrast is observed between wet soils and dry soils.

*Near infrared (0.85 ÷ 1.5 μm)* – Vegetation reduces its strong reflectivity a little; water reaches its opacity. The contrast between wet soils and dry soils becomes accentuated.

*Transition infrared (1.5 ÷ 3 μm)* – This is a domain of very good atmosphere transparency and lack of scattering. Objects appear with very sharp contours. Wet soils and dry soils contrast even more.

Sources of heat at medium-high temperature (for example lava flows) begin to be recognizable.

*Thermal infrared (3.5 ÷ 14 μm)* – This is the domain of heat emission.

## 2. Some operative applications of remote sensing

### 2.1. *Monitoring of waste disposal sites*

The monitoring of waste disposal sites is important for two main reasons:

a – To check that the biogas, produced by anaerobic digestion and being explosive, is kept confined within the waste disposal site.

b – To evaluate the flow of the biogas leaving the waste disposal site from the upper surface. Its knowledge accounts for the description of the cultivation system.

a – The biogas is formed by a mixture of methane, carbon dioxide and hydrogen sulphurized (roughly in the ratio of 60%, 39.5% and 0.5% respectively). Due to digestion processes, the biogas is accompanied by production of heat. A certain quantity of water vapour follows the emersion of biogas to the surface of the waste disposal site, where, merging in the atmosphere, it leaves a thermal print on the soil. By means of techniques of remote sensing, the monitoring of waste disposal sites is based mainly on the analysis of these thermal prints.

The biogas can also have an impact on vegetation, in particular on grass: the presence of a continuous, although weak, flow of biogas can alter the physical status of vegetation, which can be used as an environmental indicator. This aspect is very interesting in all cases where the path of biogas followed by the biogas to escape from the site edge is so long that it absorbs the entire heat content. When emerging at the surface the biogas cannot leave any thermal print on the soil: in such a case only the grass colonizing the areas of emersions can reveal the presence of biogas through their anomalous spectral response. It is well known that vegetation, when stressed by unfavourable environmental conditions, tends to show a drop in reflectivity in the near infrared spectrum together with some increase of reflectivity in the visible domain (mainly in the red region). Given the data in the near infrared *IRF*, blue *B*, green *G* and red *R*, the function

$$S = \text{arctg } IRF/(B + G + R)$$

describes the phytosanitary status of vegetation.

b – The evaluation of the flow rate of the biogas emerging from the soil into the atmosphere can be obtained through the heat balance in steady state. The amount of heat $Q$ introduced into the system (due to digestion) must, in steady state, balance the amount of heat dissipated at the site surface by irradiation $Q_{irr}$, convection $Q_{cv}$ and conduction $Q_c$

$$Q = Q_{irr} + Q_{cv} + Q_c .$$

The energetic link between the area of digestion where the heat is produced and the area of dis-

sipation at the soil surface is given by the transfer of heat $Q_{tr}$

$$Q_{tr} = \text{cm } (T_s - T_m)$$

with

$Q_{tr}$ heat transferred from digestion to dissipation area;
$c$ specific heat of the biogas;
$m$ biogas mass transferred;
$T_s$ temperature at digestion;
$T_m$ temperature at soil level.

Neglecting the heat exchanged by conduction, we can say

$$Q_{tr} = Q_{irr} + Q_{cv}$$

$$\text{cm } (T_s - T_m) =$$

$$= \{\varepsilon\sigma\Sigma_i A_i (T_i^4 - T_m^4) + bf(v)[\Sigma_i A_i (T_i - T_a)]\}$$

with

$c$ specific heat of the biogas;
$m$ biogas mass transferred;
$T_s$ temperature at digestion centre;
$T_m$ temperature of the indisturbed soil;
$\varepsilon$ emissivity of the $A_i$ areas (thermal prints at the soil surface);
$\sigma$ Stefan-Boltzmann constant;
$A_i$ isothermal areas (thermal prints at the soil surface);
$T_i$ temperature of $A_i$ area;
$b$ constant;
$f(v)$ function of the wind speed $v$ at the soil surface;
$T_a$ air temperature at the soil surface (in practice equal to the temperature of undisturbed soil).

Dividing by time $t$ and resolving in terms of mass flow $m/t$, we have

$$m/t = \{\varepsilon\sigma\Sigma_i A_i (T_i^4 - T_m^4) +$$

$$+ bf(v)[\Sigma_i A_i (T_i - T_a)]\}\ c/(T_s - T_m).$$

Eventually, adopting the technical annotation of engineering and referring to biogas volume, we have

$$m/t = \{\varepsilon\ 4.96\ [\Sigma_i A_i [(T_i/100)^4 - (T_m/100)^4]] +$$

$$+ (5 + v/1100)\ [\Sigma_i A_i (T_i - T_m)]\}/\{[T_s - T_m]c\}$$

with

$m/t$ flow amount of biogas in volume [$m^3$/h];
$\varepsilon$ average value of emissivity of the soil on the whole spectrum (typically a value around 0.6);
4.96 Stefan-Boltzmann constant [Cal/$m^2$ h $K^4$];
$A_i$ isothermal areas [$m^2$];
$T_i$ temperature of $A_i$ area [K];
$T_m$ temperature of the air at the soil level, assumed equal to the average temperature of the undisturbed soil;
$v$ wind speed at the soil level [m/h]:
$T_s$ temperature at the digestion centre [K];
$c$ specific heat of the biogas [Cal/$m^3$].

Let us return to remote sensing. The values of $T_i$ and of $A_i$ are obtained by thermography. The air temperature at soil level is assumed, using always thermography, equal to the one of the «undisturbed» soil, to say, the average value of soil temperature outside the areas where the biogas emerges. Wind speed is measured at ground level at the time of the survey (it could also be estimated at the flying altitude accounting for the flight line deviation). Neglecting the heat transferred from the soil surface to the atmosphere, with this datum we are able to compute the heat dissipation. This quantity is the final datum furnished by remote sensing. From that standpoint, any conclusion on the biogas flow must pass through the introduction of two additional unknowns: the digestion temperature $T_s$ and the value of specific heat $c$ of the biogas. The temperature of digestion varies with environmental conditions, mainly season and rainfall. For the value of biogas specific heat $c$ of the biogas can be taken as the total heat contained in the saturated water vapour which accompanies it.

The observation that the biogas emerges at the soil surface together with saturated water vapour suggests the introduction of the total heat contained in the water vapour as an acceptable value. For example, assuming that the digestion occurs at 35 °C, we can take for c the value of 25 [Cal/$m^3$].

Thus a typical structure of the equation for the most common situations in Northern Italy, with neglectable wind speed, average value of the emissivity of the soil 0.6 and digestion tem-

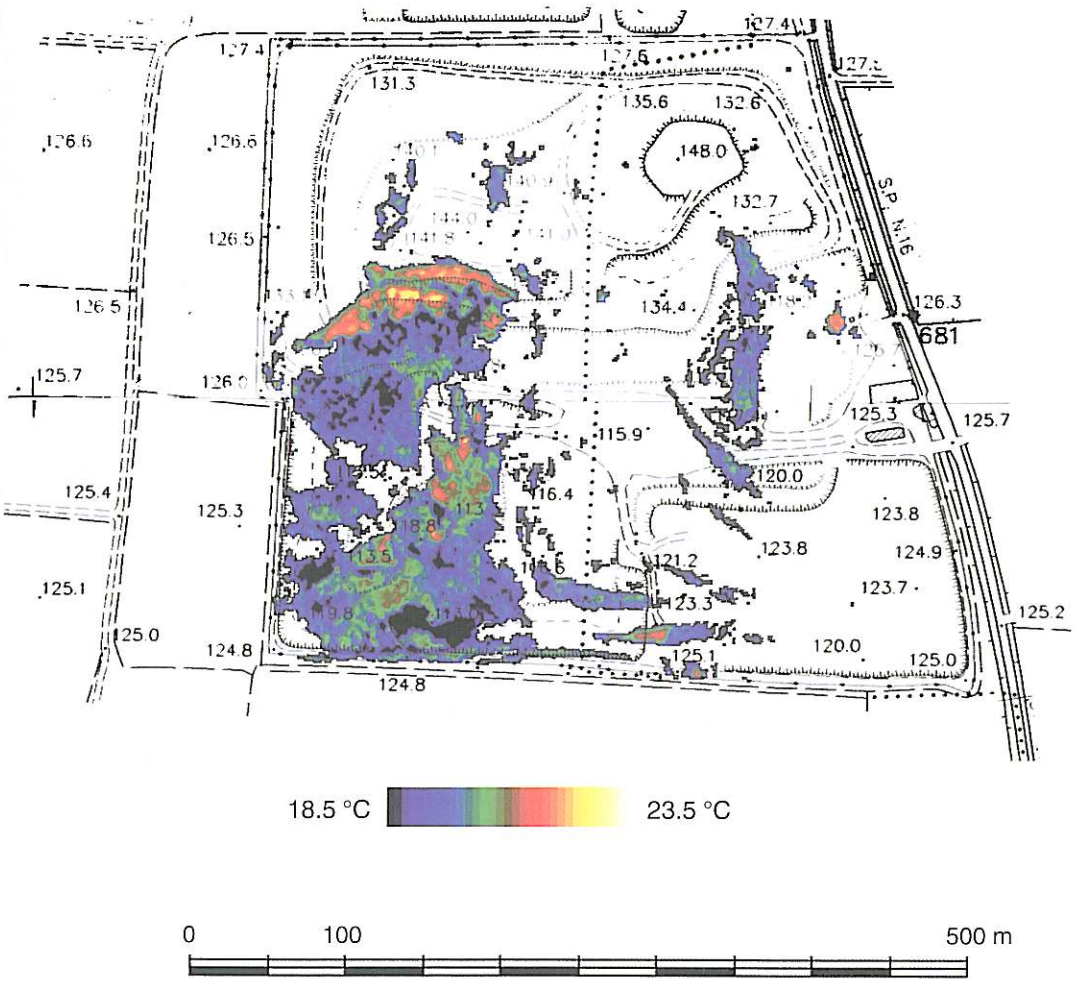


**Fig. 2.** Monitoring of waste disposal sites. Report on a topographic base of the thermographic data gathered by aircraft. The thermal anomalies, recognized by the interpreter as due to biogas emersions – then after the removal of every extraneous source of heat – are reported with the corresponding thermal calibration in coded colours. After such an operation there are, at our disposal, the extensions of the areas $A_i$ at the temperature $T_i$ needed for the computation of the biogas flow:

$$m/t = \{\varepsilon\ 4.96\ [\Sigma_i A_i[(T_i/100)^4 - (T_m/100)^4]] + (5 + v/1100)\ [\Sigma_i A_i(T_i - T_m)]\}/\{[T_s - T_m]c\} \quad \text{(see text)}.$$

In this case, with negligible wind speed, undisturbed soil temperature $T_m$ of 18.5 °C, and digestion temperature assumed at 35 °C, a free biogas flow in an atmosphere of 278 $m^3$/h was found. According to the observation that the digestion to produce 1 $m^3$ of methane is accompanied by the release of about 1750 Cal, the evaluation of methane flow could be estimated just dividing the heat dissipated at the waste disposal site surface by that specific value. As is obvious, the very first approach using thermal data consists of looking for possible existing escape routes for the biogas from the fences of the disposal site. In the example no biogas escapes are recognized.

perature of 35 °C is

$$\text{flow } [m^3/h] = \{0.6 \times 4.96\ [\Sigma_i A_i [(T_i/100)^4 - (T_m/100)^4]] + (5)\ [\Sigma_i A_i (T_i - T_m)]\}/[(T_s - T_m)25].$$

Recently, according to the numerous observations that the generation of 1 $m^3$ of methane in the most common environmental conditions of the waste disposal sites is associated with the production of about 1750 Cal, the methane flow is evaluated dividing the heat dissipated at the soil surface by that specific value.

Figure 2 shows the report on a topographic base of thermographic data gathered by aircraft on a waste disposal site. The thermal anomalies, recognized by the interpreter as due to biogas emersions – then after the removal of every extraneous source of heat – are reported with the corresponding thermal calibration in coded colours. After such an operation there are, at our disposal, the extensions of the areas $A_i$ at the temperature $T_i$ needed for the computation of the biogas flow. In this case, with negligible wind speed, undisturbed soil temperature $T_m$ of 18.5 °C, and digestion temperature assumed at 35 °C, a free biogas flow in atmosphere of 278 $m^3/h$ was found.

As is obvious, the very first approach using thermal data consists of looking for possible existing escape routes for the biogas from the fences of the disposal site. Other aspects are investigated by different techniques (see note).

*Note* – The waste disposal site is an area of anomalous electrical conductivity. Measurements performed on waste disposal sites in different zones of Northern, Central and Southern Italy have always shown an increase in electrical conductivity with respect to the bordering areas. Due either to metallic or ionic conduction, the mean conductivity within the spessor of the first few metres under the surface increases from a minimum of around 30% to values reaching 1000%. On the other hand, measurements of dielectrical constant on the same waste disposal sites have not shown any significant variation. Having considerable variation of resistivity and negligible variation of dielectric constant seems to indicate the use of radar as an interesting complementary tool, also from space, to recognize the location of old sites of uncontrolled discharge of wastes.

### 2.2. *Contribution of remote sensing to the analysis of slope stability*

In planning interventions to remove unstable blocks from rocky walls and to design works for mitigating the consequences of fall of stones, it is important to acquire a general overview of the situation and characteristics of the rocky wall.

With techniques of remote sensing some particular information can be acquired to assist intervention engineering. There are three contributions we are going to discuss:

a – The probable relative age of the detaching niches.

b – The distribution of fractures and their density.

c – The intrusion of water.

a – It has been observed, at least with respect to calcareous formations, that a recent detaching surface is associated with
– higher colour saturation than the ones long since exposed to wheatering;
– the trend of no polarizing of light (amorphous behaviour);
– often phoenomena of luminescence.

The saturation of a colour image, whose components are blue $B$, green $G$ and red $R$, is given pixel by pixel $(x, y)$ by the relation

$$S(x, y) = 1 - g(x, y)/a(x, y)$$

with

$S$ saturation;
$g$ minimum intensity value among $B$, $G$ and $R$;
$a$ average value of $B$, $G$ and $R$.

It was observed that the saturation of surface colour, at least on calcareous formations, decreases over time with wheatering.

The property of polarizing the incident light changes also with the exposiure of rocky surfaces to wheatering. Nevertheless, such a phenomenon is neither regular nor really evident and could lead to misinterpretation. In synthesis, it can be said that the general trend of a rocky surface is that of becoming even more «gray», and often glossy too, with exposure over time to wheatering factors.

Luminescence phenomena often take place on surfaces of detachment. Luminescence on the surface of a fracture loses strength with weathering. Then luminescence can be adopted just to contribute to the description of the temporal succession of detachments from a rocky wall.

For our application, luminescence means emission in the visible range under the stimulation in the ultraviolet region. In the operative situation of a rocky wall, the illumination by ultraviolet radiation of the wall itself in the darkness to stimulate the emission in the visible spectrum cannot be proposed. One way to overcome this difficulty consists of the exploitation of the variation of sun irradiance spectrum in the transitory phase. For example, during the sun illumination transitory of the morning the relative amount of intensity of ultraviolet, with respect to the amount of visible, increases greatly approaching midday.

In fact, the stimulation of luminescence by ultraviolet radiation can be studied by means of multitemporal surveys in the visible domain. Given a surface to analyse, let us perform two surveys at the subsequent times $t_1$ and $t_2$, for example during the transitory of increasing illumination. The relative amount of ultraviolet *UV*, blue *B*, green *G*, red *R*, changes according to the differential absorption of the atmosphere. If we provide two surfaces of reference for calibrating the colour, the former dark gray, the latter light gray, we could arrange the images collected at the times $t_1$ and $t_2$, respectively, to have the same value of blue *B*, green *G* and red *R* on the reference surface. This operation is intended to compensate the composition of visible light passing from the situation at time $t_1$ to the one of $t_2$. If no stimulation of luminescence exists on the surface, performing the difference of the images, band by band, zero would be obtained. On the contrary, if a stimulated luminescence exists, its effect would be that of being added to the reflection. The steps of the procedure are the following:

– Calibration of the response of blue *B*, green *G* and red *R* on the reference surface *R*1 dark gray and *R*2 bright gray

$$B_{R1}(t_1) = \gamma_B[B_{R1}(t_2) + c_B]$$
$$B_{R2}(t_1) = \gamma_B[B_{R2}(t_2) + c_B]$$
$$G_{R1}(t_1) = \gamma_G[G_{R1}(t_2) + c_G]$$
$$G_{R2}(t_1) = \gamma_G[G_{R2}(t_2) + c_G]$$
$$R_{R1}(t_1) = \gamma_R[R_{R1}(t_2) + c_R]$$
$$R_{R2}(t_1) = \gamma_R[R_{R2}(t_2) + c_R]$$

where

*B*, *G*, *R* are the three blue, green and red components;
*R*1, *R*2 are the two references;
$\gamma$, *c* are parameters (contrast and brightness).

– Once $\gamma$ and *c* are obtained on the references *R*1 and *R*2 (thus null difference on the same), a «compensated» image is obtained and the difference on the other picture elements of the image will not be null if the phenomenon of luminescence has taken place. The difference

$L =$ image $(t_2)$ – image compensated $(t_1)$

then

$$L_R = R(t_1) - \gamma_R[R(t_2) + c_R]$$
$$L_G = G(t_1) - \gamma_G[G(t_2) + c_G]$$
$$L_B = B(t_1) - \gamma_B[B(t_2) + c_B]$$

would reveal luminescence and furnish the relevant components. In general, just the brightness of the image composed by $L_R$, $L_G$, $L_B$, is considered to disclose the location and intensity of luminescence (see fig. 3, upper right, where the most recent detachment niches appear characterized by a stronger luminescence).

b – In relation to rock fractures analysis, it can be observed that any mechanical discontinuity on a surface tends to produce the polarization of incident light. The presence of polarization can be enhanced comparing images collected under orthogonal planes using a rotating polarizing filter (see fig. 4). For any pair of conjugate angles $\alpha$, $\alpha + \pi/2$ of the filter rotation, the images would show the same intensity of reflection on every pixel if no polarization occurs. If, on the contrary, there is some polarization, on these points the intensity of reflection would change with the orientation of the polarizing filter.

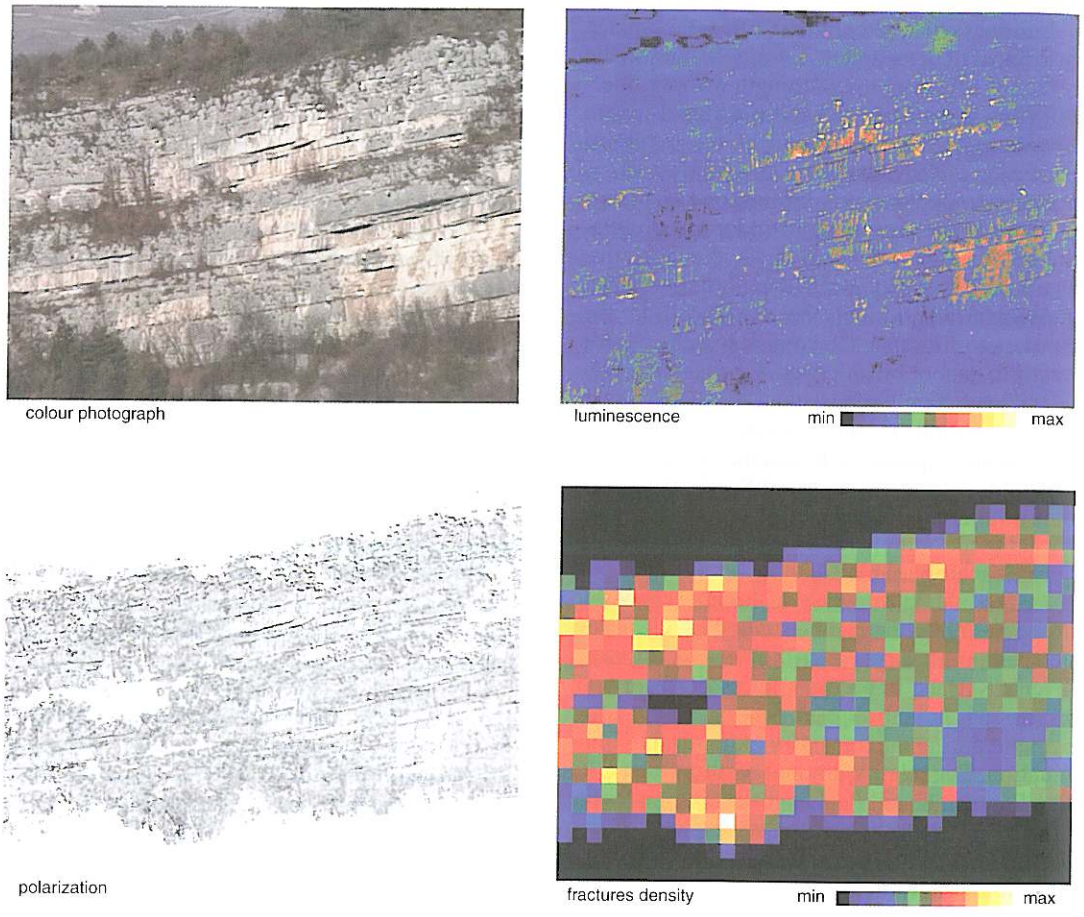


**Fig. 3.** Analysis of a rocky wall. *Upper left*: picture of a frame of a rocky wall. With the help of a digital TV camera a multitemporal series of images in the increasing illumination transitory (at 09.30 a.m and 10.30 a.m., respectively) was taken as well as a series of multipolarization images with the subsequent position $\alpha$, $\alpha + \pi/4$, $\alpha + \pi/2$, $\alpha + 3/4\pi$ of a rotating polarizing filter put in front of the TV camera objective. *Upper right*: luminescence phenomena accompanying the detachment niches. The scale reports the intensity of the phenomenon. The most recent niches are characterized by a stronger luminescence. The analysis has been performed comparing the intensities of the image collected at time $t_2$ with the one, compensated, collected at time $t_1$: $L$ = image ($t_2$) – image compensated ($t_1$) (see text). *Lower left*: result of the polarization analysis, to enhance the fractures, carried out using the formula: $P'$ = arctg min/max (see text). In the code of representation, the mechanical discontinuities, and then the fractures (corresponding to polarization, then with arctg $< \pi/4$), appear in dark gray tones on bright background. The vegetation has been removed from the frame using a proper mask. *Lower right*: distribution of the density of fractures on squares of $2 \times 2$ m$^2$ according to a conventional colour coded scale.

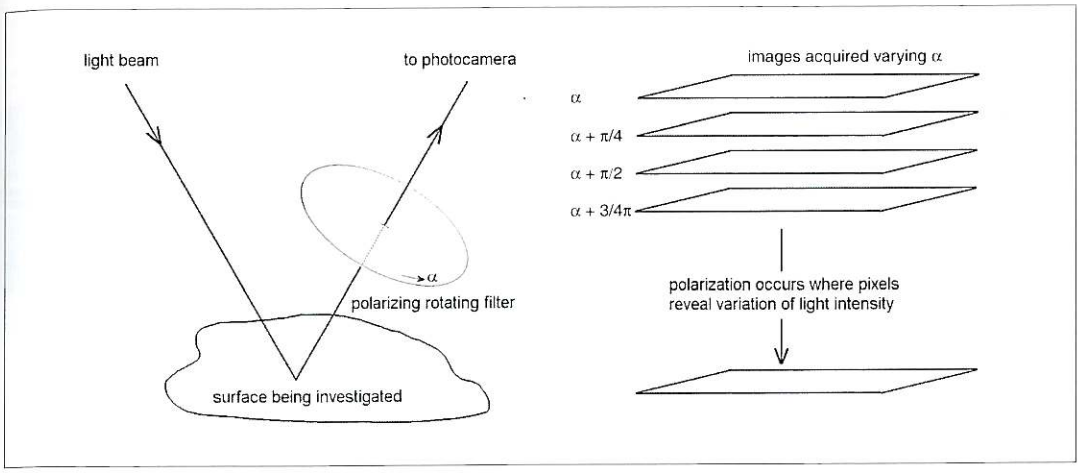


**Fig. 4.** To analyze the polarizing property of a surface, a series of images are collected in the visible range by a photocamera fitted with a rotating polarizing filter. If, on the same target, 4 frames are collected each by the rotation of a polarizing plane of $\pi/4$, point by point exhibiting the same intensity as the reflected light, no polarization phenomenon occurs. Otherwise polarization is revealed, like that associated to any mechanical discontinuity on the surface under investigation.

To describe the polarization the following formulation can be proposed:

$$P = |\log R(\alpha, x, y) - \log R(\alpha + \pi/2, x, y)| +$$

$$+ |\log R(\alpha + \pi/4, x, y) - \log R(\alpha + 3/4\pi, x, y)|$$

with

$P$ intensity of polarization;
$R$ intensity of reflection at the general pixel $(x, y)$ as collected according the polarizing planes $\alpha$, $\alpha + \pi/4$, $\alpha + \pi/2$, $\alpha + 3/4\pi$.

The idea of using log is suggested to compensate the morphological impact of the surface being investigated and then to smooth the highest values.

Another proposal for the comparison of reflection intensity under different polarization planes is given by the collection of a series of $n$ images along with a continuous rotation of a polarizing mirror between $\alpha$ and $\alpha + \pi/2$. The $n$ images will admit, pixel by pixel, a maximum and a minimum for the reflection strength only if polarization takes place. The following procedure could be suggested:

– Collection of $n$ images with the rotation of a polarizing filter within $\alpha$ and $\alpha + \pi/2$, possibly with a uniform step of $(\alpha + p\ \pi/2)$ with $p = \pi/2n$;

– Computing, pixel by pixel on the $n$ images, of the minimum min and the maximum max;

– Computing of

$$P' = \text{arctg (min/max)}.$$

Values of $P' < \pi/4$ are found where polarization occurs. The function arctg is introduced to «linearize» the ratio itself (see fig. 3, lower left, where the fractures appear in dark gray tones on bright background. In fig. 3 lower right the distribution of fractures density on squares of $2 \times 2$ m$^2$, according to a conventional colour coded scale, is shown).

c – The study of the heat capacity of a rocky wall is of worth to recognize either the areas with high humidity content (high heat capacity) or the densely fracturated ones (low heat capacity).

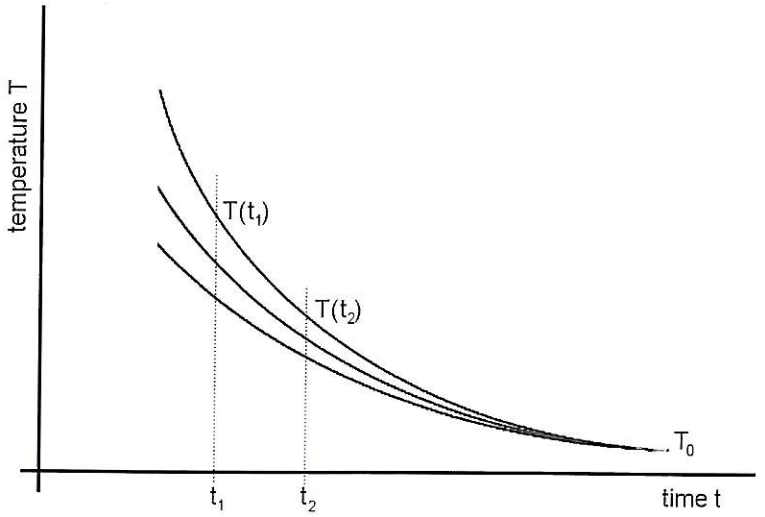


**Fig. 5.** In the cooling down transitory, with negligible illuminating radiation, materials with different heat capacity show a different temperature drop. Lower slopes of the curve $T(t)$ belong to materials with high specific heat. The thermal transitory starts from the thermal level each material has reached according to its own energization conditions, which, in turn, depend on the surface morphology. To compute the heat capacity the hypothesis of an asymptotic trend of all materials to a common $T_0$ value is introduced.

In the thermal surveys by ground fixed stations, the heat capacity can be evaluated exploiting the thermal transitory in the cooling down phase (see fig. 5). According to Newton's law which describes the temperature drop with the time in the cooling transitory, we say

$$T(t) - T(t_3) = [T(t_1) - T(t_3)]e^{-(hSt/cm)}$$

with

- $T(t)$ temperature at instant $t$;
- $T(t_3)$ final temperature (end of transitory);
- $T(t_1)$ temperature at the beginning of transitory;
- $h$ thermal adduction coefficient $h$ (accounting for emission and convection);
- $S$ unity area (in our case, area of the pixel of the thermal image);
- $t$ time;
- $c$ specific heat;
- $m$ mass.

Rendering the expression explicit in the heat capacity $cm$, we obtain

$$cm = hSt/\ln\{[T(t_1) - T(t_3)]/[T(t) - T(t_3)]\}.$$

In the commonest case, the variations of the adduction coefficient $h$ on the surface of rocky walls are negligible and its value can be substituted by a constant. The area $S$ is also constant and, in our case, corresponds to the image element (pixel). The final temperature $T(t_3)$ is, practically, an asymptotic value and can be substituted with another constant $T_0$.

Thus collecting two temporal series of thermal images $T(t_1)$ and $T(t_2)$, we eventually obtain

$$cm = B_0/\ln\{[T(t_1) - T_0]/[T(t_2) - T_0]\}$$

with

- $cm$ heat capacity;
- $B_0$ constant (in practice, a factor of visualization for the image);
- $T(t_1)$ temperature at time $t_1$ (around the beginning of transitory);
- $T(t_2)$ temperature at a subsequent time $t_2$;
- $T_0$ constant accounting for the final temperature (end of transitory).

Figure 6 presents the investigation of heat ca-

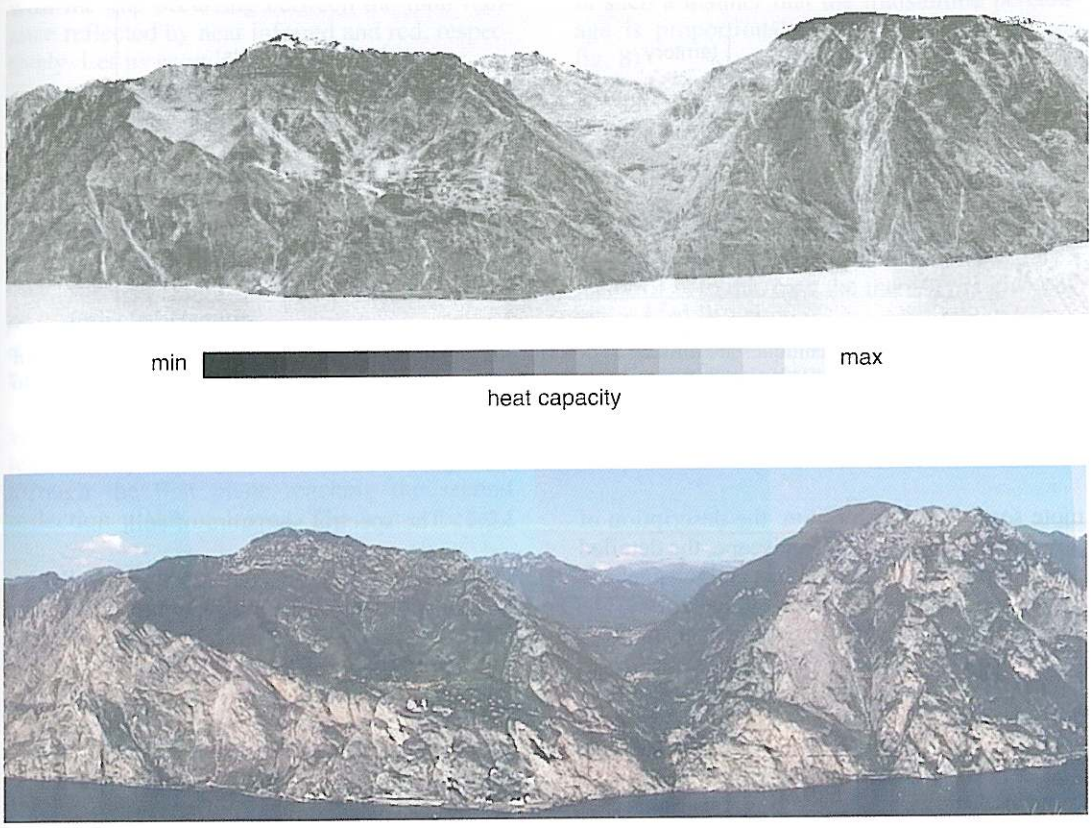


**Fig. 6.** Analysis of a slope. *Above:* series of rocky walls investigated to describe, among other aspects, the moisture content and the density of fracturation. The analysis has been carried out computing the heat capacity, exploiting the cooling down thermal transitory of the evening. The heat capacity, given on a defined pixel by the product of specific heat $c$ by the density of the mass $m$ associated to the pixel itself, is described, collecting two temporal series of thermal images $T(t_1)$ and $T(t_2)$, by the formula: $cm = B_0 / \ln\{[T(t_1) - T_0]/[T(t_2) - T_0]\}$, with $cm$ = heat capacity; $B_0$ = constant (in practice, a factor of visualization for the image); $T(t_1)$ = temperature at time $t_1$ (around the beginning of transitory); $T(t_2)$ = temperature at a subsequent time $t_2$; $T_0$ = constant accounting for the final temperature (end of transitory) (see text). We are along the shores of a big lake. The scale reports by means of a code of grey tones the distribution of the heat capacity. *Below*: the comparison with the image collected in the visible gives an idea on the lot of information concerning drainage, moisture and fractures which can be acquired from the distribution of heat capacity.

pacity on a series of rocky walls (above) in a gray scale code with the corresponding image collected in the visible (below). The comparison between the two images gives an idea of the amount of information concerning drainage, moisture and fractures which can be acquired from the distribution of heat capacity.

## 3. Remote sensing and archaeological prospecting

### 3.1. *General introduction*

There are three principal items of archaeological interest to which the techniques of re-

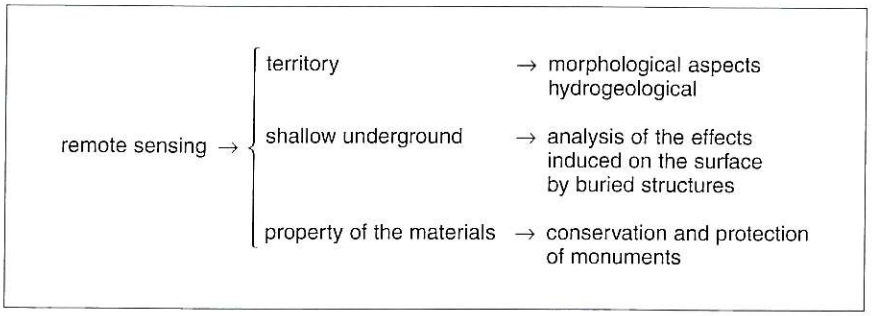


**Fig. 7.** Remote sensing techniques are utilized to describe the general hydrogeological environment of areas of potential archaeological meaning to investigate on the soil subsurface and, in dwellings and monuments, to identify inhomogeneities inside structures, damage, humidity retention and other phenomena.

mote sensing can contribute: the description of physiographic aspects of landscape, the detailed prospecting of buried remnants and the analysis of the conservative status of monuments.

Let us try to synthetize with the help of fig. 7.

The first point concerns the description of the landscape morphology, with its hydrogeological aspects, and the inventory of resources. The second is aimed at the search for buried anthropic structures, exploiting the impact of mechanical discontinuities at the soil surface. The third point regards the description of monuments from the point of view of the geometry, types of building materials, status of conservation, results of interventions, and so forth.

### 3.2. *Vectors of information*

The irregular distribution of humidity on the soil surface could be an indicator of the non-uniformity of the shallow underground. The humidity modulates the colour of the bare soil, the density and status of vegetation, the heat capacity and heat conductivity as well as the dielectric constant and electrical conductivity.

The aim of remote sensing in archaeological investigations is the detection of those aspects of the shapes of humidity distribution, revealed at the soil surface, which could be related to buried remnants of anthropic settlements.

#### 3.2.1. The spectral signature of soil

The colour of soil, and more generally its spectral signature, varies with composition and content of superficial humidity. If dry, the soil appears brighter and brighter as the wavelength of the illuminating source sweeps from the region of blue (0.4 $\mu$m) to the one of near infrared (around 1 $\mu$m and beyond); if, wet, the soil appears as less bright as the wavelength increases beginning from the region of red (0.7 $\mu$m).

#### 3.2.2. Vegetation as an indicator

Density and physical status of vegetation can provide us by useful information on the permeability of the upper spessor of soil. Their distribution on the soil surface can reveal patterns characterized by peculiar shapes, of significance to archaeologists. In practice, it is possible to observe a lower density and a worse status above remnants of masonry where the soil has a reduced thickness.

Grass, in a normal situation, reflects very little in the blue region (2% or less), on the average in the green (around 15%), few in the red (around 6%) and strongly in the near infrared (40% and more). A peculiar behaviour of vegetation is that of transmitting an amount of radiation proportional to the reflected one. As a global effect, the density of vegetation increases

with the gap occurring between the total radiance reflected by near infrared and red, respectively. Let us examine this point.

According to the law of Kirchhoff on the conservation of energy

$$1 = \rho + \alpha + \tau$$

with

1 unitary radiant energy impinging on a surface;
$\rho$ reflected fraction;
$\alpha$ absorbed fraction;
$\tau$ transmitted fraction;

vegetation reflects from the first upper plane of leaves the percentage $\rho$. The amount $\tau$ passes through the first plane reaching the second reflection plane of leaves. The leaves behave in such a manner that the transmitted percentage is proportional to the reflected one (see fig. 8)

$$\tau = k\rho.$$

Thus, by the second plane of leaves the amount $\rho\tau = k\rho^2$ is reflected. The beams reflected by the second plane with intensity $k\rho^2$, if encountering the upper plane again are attenuated by a factor of $\tau$. In this case the intensity is given by $\rho\tau\tau = k^2\rho^3$.

Stopping at this point of the multiple playing of reflection and transmission, then just accounting for the primary reflection from the upper plane and the subordinate reflection from a second plane, the sensor will collect

$$\rho_{tot} = \rho + k\rho^2 + k^2\rho^3$$

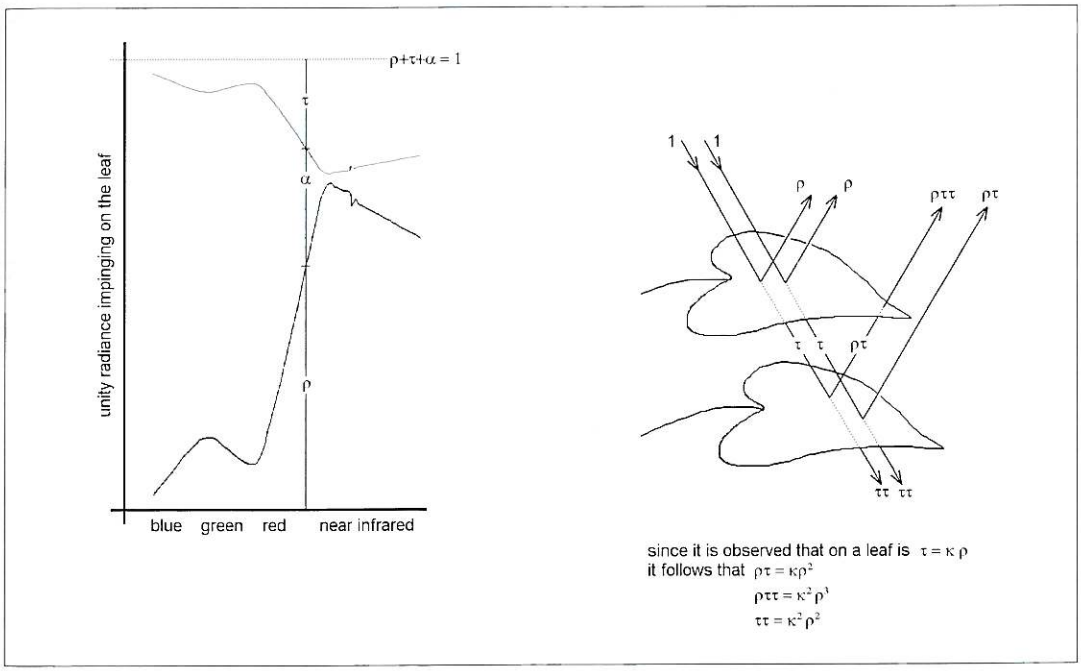


**Fig. 8.** According to the energy balance (Kirchhoff law), the unity radiance impinging on leaves (1) is in part reflected ($\rho$), in part transmitted ($\tau$) and then in part absorbed ($\alpha$). Due to the peculiar property of leaves to have transmission $\tau$ proportional to reflection $\rho$, the global effect is that of increasing the difference between the reflection intensity in the region of near infrared (high value) and in the region of red (low value) as the amount of leaves involved increases. Thus such a difference increases with the biomass.

with

$\rho_{tot}$ global reflected radiant energy impinging on multiplane leaves system;

$k$ proportionality factor.

The percentage $\rho_{tot}$ is higher than $\rho$. Comparing data collected in a high reflectivity spectral domain, like near infrared $\rho_{irf}$, with another collected in a low reflectivity spectral range, like red $\rho_r$, we obtain

$$\rho_{tot\,irf} - \rho_{tot\,r} =$$

$$= \rho_{irf} + k\rho_{irf}^2 + k^2\rho_{irf}^3 - (\rho_r + k\rho_r^2 + k^2\rho_r^3) =$$

$$= (\rho_{irf} - \rho_r) + k(\rho_{irf}^2 - \rho_r^2) + k^2(\rho_{irf}^3 - \rho_r^3).$$

Clearly, it is

$$\rho_{tot\,irf} - \rho_{tot\,r} > \rho_{irf} - \rho_r$$

$k$ being a positive value and

$$\rho_{irf}^2 > \rho_r^2 \quad \text{and} \quad \rho_{irf}^3 > \rho_r^3.$$

The gap clearly increases with the order $n$ of leaves reflecting planes. Thus we can, in general, report

$$\rho_{tot\,irf} - \rho_{tot\,r} = \sum_{i}^{n} k^{i-1}(\rho_{irf}^i - \rho_r^i).$$

As a consequence, the density of leaves can be described with formulas comparing the intensity of reflection in the domain of near infrared *IRF* and red *R* respectively. In order to remove the influence of the orientation of the reflecting planes, the comparison has to be normalized to a quantity showing the same angular dependence like

normalized density vegetation index
$NDVI = (IRF - R)/(IRF + R)$

density of vegetation
$D = \text{arctg } IRF/R.$

By means of a somewhat similar analysis, the relation defining the physical status of vegetation $S$ is obtained using the bands of near infrared *IRF*, red *R*, green *G* and blue *B*

physical vegetation status
$S = \text{arctg } IRF/(B + G + R).$

**Fig. 9.** A general purpose analysis on land. *Upper left*: colour picture of a frame of land of about 3 hectares. *Upper right*: corresponding false colour photograph taken using Kodak Ektachrome infrared professional EIR film provided with a Wratten 12 yellow filter. It obtains the colour conversion

| *Original spectral interval* | *Colour attributed* |
|---|---|
| near infrared (0.7 ÷ 0.85 $\mu$m) *IRF* | red |
| red (0.6 ÷ 0.7 $\mu$m) *R* | green |
| green (0.5 ÷ 0.6 $\mu$m) *G* | blue |
| blue (0.4 ÷ 0.5 $\mu$m) *B* | black |

Vegetation appears with a red-magenta aspect, while bare soil shows a grey-cyan hue. *Middle left*: computing of the density of vegetation (biomass) by means of the relationship: $D = \text{arctg } IRF/R$. Note the higher density in the lower left corner of the frame. *Middle right*: computing of luminescence by comparison of two subsequent surveys carried out in the phase of increasing illumination transitory (see text). Note the different response of the bare soil in the upper and lower part of the field. *Lower left*: distribution of the temperature as reported by a thermographic survey carried out in the increasing thermal transitory of the morning. In the code of representation the temperature increases from dark to light grey tones. Large part of the bare soil appears much moistened (combined effect of higher heat capacity and cooling due to evaporation). *Lower right*: distribution of the temperature gradients on the soil surface. In the code of representation the temperature gradient increases from dark to light grey tones according to the formula: $G = \text{arctg min/max}$, with $G$ = temperature gradient; min, max = minimum and maximum value of temperature on 2×2 pixel matrix. Low gradient could correspond to higher thermal conductivity areas. This is an example of a general first approach to study an area of potential archaeological interest with the help of remote sensing techniques.

colour photograph

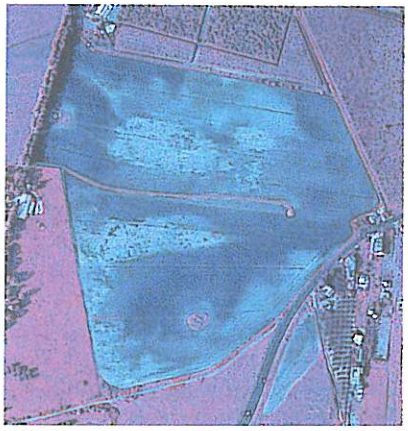

false colour infrared photograph

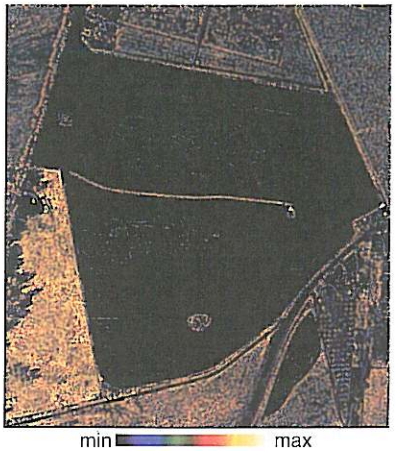

min max

biomass

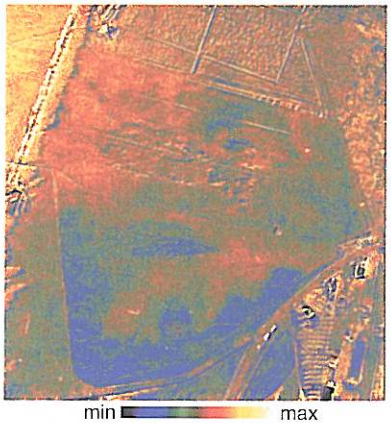

min max

luminescence

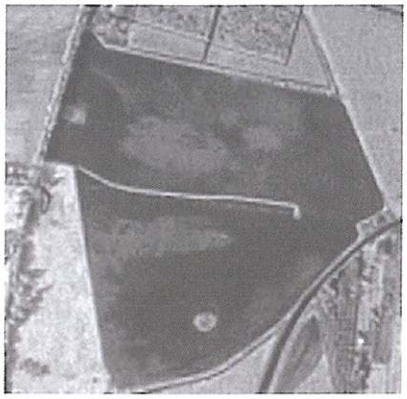

thermography

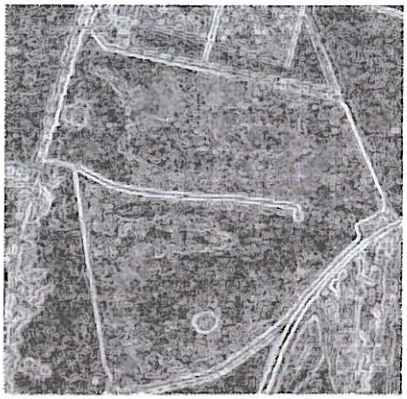

thermal gradients

3.2.3. Thermal parameters

Due to the phenomenon of capillarity, the water stored within the soil mass is conveyed to the soil surface, where evaporation produces a local temperature drop and then a thermal print. The presence of water shows its effect on other properties of the soil mass, like heat capacity and heat conductivity.

The heat capacity can be adopted as an index of the water content of the soil and then to recognize more or less permeable materials. The heat capacity as well as the heat conductivity increase with the content of water. In synthesis, the areal distribution of temperature, heat capacity and heat conductivity, are means of major importance in the field of archaeology in all cases in which moisture content can be significant seepage of a buried discontinuity both on soil and monuments.

3.3. *Other aspects of the surfaces: luminescence, polarization, roughness*

Sometimes, to the radiance reflected by a given surface another quantity is added due to luminescence stimulated by ultraviolet radiation. The phenomenon can have a considerable importance in the analysis of soils and walls. In fact, traces of strange materials (like bricks, stones, and so forth) pushed to the surface by cultivation work can be revealed through their different luminescence. The same happens in some cases analysing parts of monuments where the use of materials of different origin can be detected.

Polarization and roughness are additional aspects to describe a surface from the point of view of being more or less glossy or mat, polished or rough, although of the same colour. These aspects, which can be enhanced using proper approaches of processing on remotely sensed data, are useful to define alterations on a surface.

Figure 9 presents an example of the general first approach to study an area of potential archaeological interest with the help of remote sensing facilities. In the upper left position is the colour picture of a frame of land of about 3 hectares collected by aircraft while on the right we have the corresponding false colour photograph taken using Kodak Ektachrome infrared professional EIR film provided with a Wratten 12 yellow filter. It obtains the colour conversion

| *Original spectral interval* | *Colour attributed* |
|---|---|
| near infrared (0.7 ÷ 0.85 $\mu$m) *IRF* | red |
| red (0.6 ÷ 0.7 $\mu$m) *R* | green |
| green (0.5 ÷ 0.6 $\mu$m) *G* | blue |
| blue (0.4 ÷ 0.5 $\mu$m) *B* | black |

Vegetation appears with a red-magenta aspect, while bare soil shows a grey-cyan hue.

On middle left the result of vegetation density computing according to the formula

$$D = \text{arctg } IRF/R$$

is presented using a colour coded scale. Note the higher density in the lower left corner of the frame.

On middle right it is depicted the computing of luminescence obtained comparing two subsequent surveys carried out in the phase of increasing illumination transitory. Note the different response of the bare soil in the upper and lower parts of the field.

The lower left of the figure shows the distribution of the temperature as reported by a thermographic survey carried out in the increasing thermal transitory of the morning. In the code of representation the temperature increases from dark to light grey tones. Much of the bare soil appears much moistened (combined effect of higher heat capacity and cooling due to evaporation).

The lower right shows the distribution of the surface temperature gradients on the soil. In the code of representation the temperature gradient increases from dark to light grey tones according to the formula

$$G = \text{arctg min/max}$$

with

| | |
|---|---|
| *G* | temperature gradient; |
| min, max | minimum and maximum value of temperature on 2×2 pixel matrix. |

Low gradient could correspond to higher thermal conductivity areas.

## 4. Contribution of remote sensing to the analysis of soil moisture

### 4.1. *Analysis of moisture on flat areas*

Superficial and mass moisture are analyzed exploiting different phenomena. For the study of superficial moisture on bare soils bands of reflection are basically used according to the observation that wet soil appears less bright as the wavelength increases beginning from the region of red. The distribution of mass moisture can be revealed using vegetation as an environmental indicator. Nevertheless, the most general way to analyse the distribution of mass moisture, practically applicable in all cases, is given by the study of heat capacity (see fig. 10), water being a vehicle with a very high specific heat. As previously presented, having two subsequent thermal surveys at our disposal, performed in the cooling down transitory, the heat capacity can be determined. On reasonably flat surfaces, with a uniform energization by the light, a most common approach to evaluate the heat capacity can be applied. Given data collected during the warming up transitory at the time $t_1$ and $t_2$, respectively, in condition of constant coalbedo, the heat capacity is defined by the relation

$$cm = Q/(T_{t2} - T_{t1}) = \text{coalb}\ (t_2 - t_1)/(T_{t2} - T_{t1})$$

with

- $cm$ heat capacity (product of specific heat $c$ by mass $m$ of the volume of material considered);
- $Q$ heat absorbed between the instants $t_1$ and $t_2$;
- coalb coalbedo (the «negative» of reflected radiance, then the radiance absorbed);
- $T_{t2}$, $T_{t1}$ temperatures of mass $m$ at the instants $t_1$ and $t_2$.

The relation can be simplified allowing the computation of heat capacity with just one survey at the time $t = t_2$ in the middle of the increasing thermal transitory, whenever the hypothesis of the temperature $T_{t1}$ being uniform at the time $t_1$ can be introduced on the scene considered. $T_{t1}$

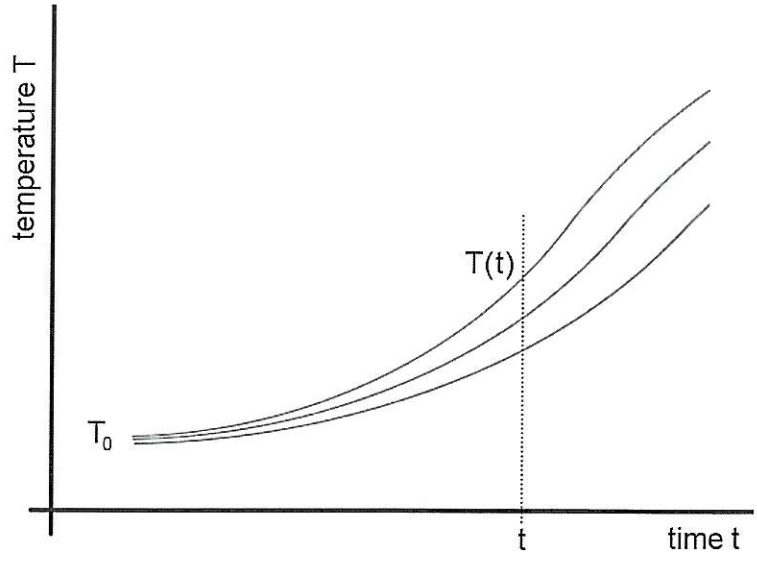


**Fig. 10.** In the increasing thermal transitory, in conditions of uniform energization, materials with different heat capacity warm up at different speeds. The rise of the curve $T(t)$ for material with high humidity content is low.

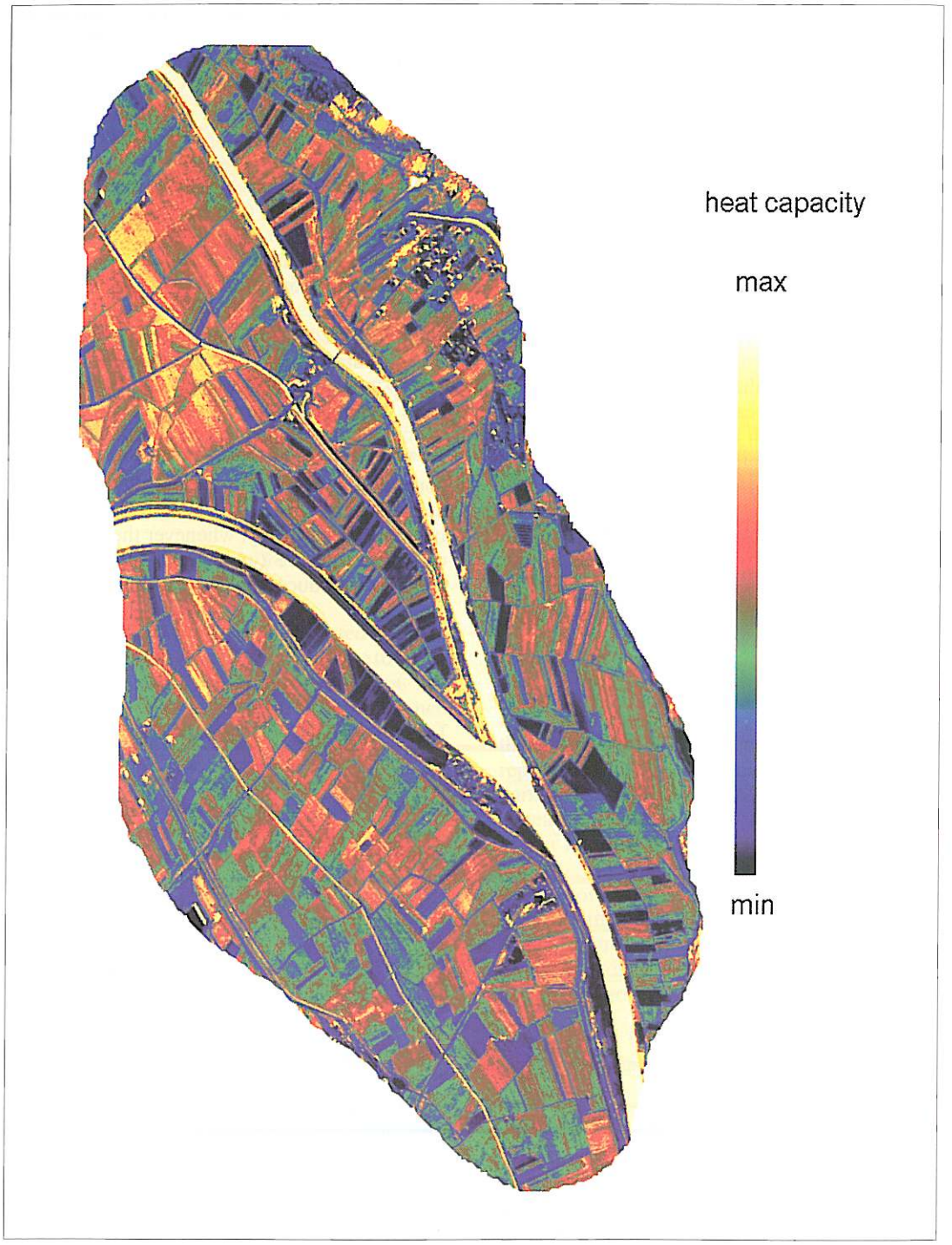
heat capacity
max
min

is then replaceable by a constant = $T_0$

$$cm = Q/(T_{t2} - T_{t1}) \approx \text{coalb}_{t2}\, k/(T_{t2} - T_0)$$

with

$cm$ heat capacity;
$Q$ heat absorbed between the instants $t_1$ (end of night) and $t_2$ (middle of increasing thermal transitory of the morning);
coalb coalbedo;
$T_{t2}$ temperature at the moment of the survey;
$T_{t1}$ temperature at the end of the night assumed as a constant = $T_0$;
$k$ constant.

For an example, with data of Landsat Thematic Mapper (which are collected in the morning around 09.30 a.m.) at our disposal, then in the situation of increasing thermal transitory, $T_{t1} = T_0$ is chosen, in practice, as the minimum temperature present on the scene diminished to a small quantity (also to avoid division by zero). We could suggest choosing a quantity around one tenth of the whole dynamic range, expressed, on the scene itself, by $T_{max} - T_{min}$. Eventually we obtain

$$cm = \text{coalb}_{t2}\, k/(T_{t2} - T_0) =$$

$$= \text{coalb}_{t2}\, k/\{T_{t2} - [T_{min} - 0.1(T_{max} - T_{min})]\}$$

and denominating with $b_2$, $b_3$, $b_4$, $b_6$ the intensities of the bands of the Thematic Mapper in the regions of green, red, near infrared and thermal infrared, respectively, we write

$$cm =$$

$$= [765 - (b_2 + b_3 + b_4)]h/\{b_6 - [b_{6\,min} - 0.1(b_{6\,max} - b_{6\,min})]\}$$

with

$cm$ heat capacity;
765 $3 \times 255$ (255 being the maximum value each band intensity can reach in the system with 8 bit). The coalbedo is then given by the complement of the albedo $(b_2 + b_3 + b_4)$;
$h$ constant for the image representation.

A similar procedure can be applied to any multispectral survey, whenever the condition of uniform illumination (then, energization) and increasing thermal transitory is satisfied. Figure 11 presents the environment of the confluence of two rivers, depicted by means of the distribution of heat capacity. In this actual case of a flat surface, the heat capacity has been evaluated using just one survey performed in the middle morning by aircraft with the hyperspectral scanner Daedalus MIVIS of Consiglio Nazionale delle Ricerche, the Italian research agency.

**Fig. 11.** Hydrogeological aspects. Environment of the confluence of two rivers, depicted by means of the distribution of heat capacity. Heat capacity can be used to analyse the moisture content of soils and then their permeability. In this actual case of a flat surface, the heat capacity has been evaluated using just one survey performed in the mid morning. Within the increasing thermal transitory, the simplified formulation can be used valid to introduce the hypothesis of the temperature $T_{t1}$ at the time $t_1$, on the whole scene being uniform, and then replaceable by a constant = $T_0$

$$cm = Q/(T_{t2} - T_{t1}) \approx \text{coalb}_{t2}\, k/(T_{t2} - T_0)$$

with $cm$ = heat capacity; $Q$ = heat absorbed between the instants $t_1$ (end of night) and $t_2$ (middle of increasing thermal transitory of the morning); coalb = coalbedo; $T_{t2}$ = temperature at the time of survey; $T_{t1}$ = temperature at the end of night, assumed as a constant = $T_0$; $k$ = general constant for the image representation. The survey was carried out by aircraft with the hyperspectral scanner Daedalus MIVIS of «Consiglio Nazionale delle Ricerche», the Italian research agency. The coalbedo was computed adding the «negative» of the 12 bands of visible. The difference $(T_{t2} - T_0)$ is given by the actual value $T_{t2}$ of thermal emission in the thermal band «96» (9.4 ÷ 9.8 $\mu$m), minus its minimum value on the whole scene $T_{min}$ diminished by 10% of the full temperature dynamic range $(T_{max} - T_{min})$: $T_0 = [T_{min} - 0.1(T_{max} - T_{min})]$ (see text). In the merging area a zone with low heat capacity (dark blue tones in the colour coded scale adopted), due to the presence of permeable gravel, can be clearly distinguished. The most humid soils (orange-red colour) are found at the margin of conoids and along palaeo river beds.

In the merging area a zone with low heat capacity (dark blue tones in the colour coded scale adopted), due to the presence of permeable gravel, can be clearly distinguished. The most humid soils (orange-red colour) are found at the margin of conoids and along palaeo river beds.

### 4.2. *Analysis of moisture on a complex morphology surface*

The thermal information accounts for the humidity of soils being related to evaporation and heat capacity. On flat surfaces, the information is relatively easy to interpret. On the contrary, when surfaces characterized by a complex morphology are given, the inhomogeneous infiltration of the water into the soil has to be accounted for.

The amount of water absorbed by soil depends on the permeability and on the time the precipitation waters have held on the surface to allow imbibition. The time the water precipitated remains on a surface depends on the slope. Let us indicate with $\alpha$ the angle of the tangent plane in a given point of a surface receiving rain. If we indicate with $m$ the mass of a single rain drop, $g$ the gravity constant and $a$ the acceleration, we have

$$mg \operatorname{sen}\alpha = ma$$

and then the distance $s$ covered in the time $t$

$$s = \tfrac{1}{2} a t^2$$

$a$ being the acceleration.

The space $s$ projected on the horizontal is espressed by $s \cos\alpha$. Thus the unitary movement on the horizontal projection is given by

$$\cos\alpha = \tfrac{1}{2} a t^2$$

hence the the time $t$ of holding on

$$t = \sqrt{(2 \cos\alpha / g \operatorname{sen}\alpha)} = \sqrt{(2 / g \operatorname{tg}\alpha)}.$$

The function tends to infinite as a tends to $\pi/2$.

For our applications, we need a multiplicative function $f(\alpha)$ to be associated with the actual permeability of the formations. Taking the value of $t$, assumed without dimensions, we could suggest for $f(\alpha)$ a function like

$$f = 1 - 1/(1+t) = 1 - 1/(1+\sqrt{(2/g \operatorname{tg}\alpha)}).$$

This function varies between 1 and 0 as the slope varies from 0 (plane) to $\pi/2$ (vertical wall) and has to be multiplied by the estimated values of soil permeability.

The information resulting from direct reading thermography and from the computing of heat capacity has to be compared with a model of the effective water infiltration to identify the «anomalies» produced by accumulation of water.

## 5. Conclusions

Of the numerous applications of remote sensing, a few have been presented above, closer to the general theme of the 10th Course of the International School of Applied Geophysics – «shallow targets» – and to be considered operative. For this reason, attention has basically focused on ground fixed stations and flying platforms. The possibility of having different bands with proper width, polarization, multitemporal surveys performed at a scheduled day time, offers perspectives not yet available by heliosynchronous orbiting platforms. In other words, remote sensing by ground fixed stations and by flying platforms «anticipates» what orbiting platforms could do, in part, in the future.

*REFERENCES*

Issues, reports and brochures of the «*Professional Master on Remote Sensing and Natural Resources Evaluation*» held yearly by the Ministry of Foreign Affairs – Istituto Agronomico per l'Oltremare, Via Cocchi 4, 50131 Florence, Italy.